Available online at www.sciencedirect.com
SCIENCE DIRECT®
International Journal of Heat and Mass Transfer 49 (2006) 582–593
International Journal of HEAT and MASS TRANSFER
www.elsevier.com/locate/ijhmt

A numerical study of the Hampson-type miniature Joule–Thomson cryocooler

Hui Tong Chua [a,*], Xiaolin Wang [b], Hwee Yean Teo [c]

[a] School of Mechanical Engineering, University of Western Australia, MDBP M050, 35 Stirling Highway, Crawley WA 6009, Australia
[b] Department of Mechanical Engineering, National University of Singapore, 10 Kent Ridge Crescent, Singapore 119260, Singapore
[c] Office of Estate and Development, National University of Singapore, 2 Estate Office Drive, Singapore 117587, Singapore

Received 12 August 2004; received in revised form 27 August 2005
Available online 17 October 2005

Abstract

The Hampson-type miniature Joule–Thomson (J–T) cryocooler is widely used in electronic cooling. We develop the geometry model of the Hampson-type cryocooler to better understand the double helical tube-and-fin heat exchanger. The steady-state governing equations of the cryogen, helical tube and fins, and shield are solved numerically and yield good agreements with experiment data. The conventional way of simulating a Hampson-type J–T cryocooler, which is accompanied by a host of empirical correction factors, especially vis-à-vis the heat exchanger geometry could now be superseded. The effort and time spent in designing a Hampson-type J–T crycooler could be greatly reduced.

1. Introduction

Recently the Hampson-type miniature J–T cryocooler has been gaining more and more attentions. It is commonly used for thermal management of power intensive electronic devices due to its compactness, simple configuration and having no moving parts. Such a J–T cryocooler can transport the refrigeration over a fairly large distance for spot cooling at several locations. Its performance can be substantially improved by the recuperative heat exchanger which incorporates the double helical tube-and-fin configuration. Fig. 1 shows a schematic of a typical Hampson-type J–T cryocooler. Its typical dimensions are listed in Table 1.

Limited experimental and theoretical works were reported in the literature due to the complexity of its geometry and variable physical properties of the compressible working fluid. Maytal [1] performed an experimental analysis on the relationship between the pressure and operation time by using an ideal, flow regulated Hampson-type Joule–Thomson (J–T) cryocooler. However heat-and-mass transfer among the cryogen, tube wall, Dewar and mandrel were not considered in the study. A one-dimensional transient model of a J–T cryocooler was presented by Chou et al. [2,3]. The momentum and energy transport equations were incorporated in the model, but the prediction was limited because the choking of flow and the curvature effect of the helical capillary tube and fins were not considered. In addition the model adopted ideal heat transfer coefficients for the tube wall, Dewar and mandrel, which was not realistic as they were highly temperature sensitive. Chien et al. [4] further adopted this simulation onto a self-regulating J–T cryocooler. The work concentrated mainly on the investigation of a bellow control mechanism on the self-regulating Joule–Thomson (J–T) cryocooler. Recently the effectiveness, flow characteristics, heat conduction and liquefied yield fraction of a Hampson-type Joule–Thomson (J–T) cryocooler were reported [5,6]. However the affiliated formulation exhibited significant thermodynamic inconsistency and the double helical tube geometry was not considered. Instead of using the real surface area for the

* Corresponding author.
E-mail addresses: htchua@mech.uwa.edu.au (H.T. Chua), mpewx@nus.edu.sg (X. Wang), oedthy@nus.edu.sg (H.Y. Teo).

0017-9310/$ - see front matter © 2005 Elsevier Ltd. All rights reserved.
doi:10.1016/j.ijheatmasstransfer.2005.08.024

Nomenclature

A	contact area, m^2
a	primary helical radius, m
b	pitch of helical tube, m
COP	coefficient of performance
c_p	specific heat capacity, J/kg K
D	diameter, m
f	fanning friction coefficient
FOM	figure of merit
G	mass flux, kg/m^2 s
h	convective heat transfer coefficient, W/m^2 K
k	thermal conductivity, W/m K
L	heat exchanger length, m
$\dot{m}$	mass flow rate, kg/s
M	standard volume flow rate SLPM
n	number of helical tubes or fins
Pitch	helical fin pitch, m
p	pressure, Pa
Pr	Prandtl number
q	heat flux, W/cm^2
R, r	radius, m
R_{curve}	radius of curvature of capillary tube, m
Re	Reynolds number
S_{gen}	entropy generation, J/K
s	J–T primary helical direction (capillary tube), m
T	temperature, K
u	bulk mean velocity of cryogen, m/s
W	effective fin width, m
H	effective fin height, m
z	J–T primary axial direction, m
α	fin surface angle, rad
β	angle for helical fins, rad
ε	emissivity, effectiveness
μ	viscosity, N s/m^2
μ_{J-T}	Joule–Thomson coefficient, K/Pa
θ	angle for helical tube, rad
ρ	density, kg/m^3
σ	Stefan–Boltzmann constant, $W/(m^2 K^4)$

Superscripts and subscripts

1	inlet of heat exchanger
3	nozzle outlet
amb	ambient
abs	absolute
f	refrigerant inside the tube
fin	helical fins
fini	fins interior
finm	fin and metal tube
fino	fins exterior
fm	gas and tube
Hx	hydraulic diameter
i	ideal
l	return refrigerant along the fins
m	capillary tube
man	Mandrel
max	maximum
mi	capillary tube interior
min	minimum
mo	capillary tube exterior
out	outlet
sat	saturation situation
sh	shield
si	shield interior
spc1	inner spacer
spc2	outer spacer
surf	fin surface
Tot	total
v	volume

calculation of the double helical tube geometry, correction factors for the heat exchange areas were used to adjust the simulation result. The curvature effect of the helical tube and the choking of flow were also missing from the simulation.

In this paper, the sophisticated geometry model of the Hampson-type heat exchanger is presented and incorporated into the simulation model. The choking of flow in the capillary tube is also considered in the simulation. This eliminates the primary limitations embodied in those earlier works [2–6]. The performance of the Hampson-type Joule–Thomson (J–T) cryocooler in the steady state condition is predicted and compared favorably with the experimental data. The conventional way of simulating the Hampson-type Joule–Thomson (J–T) cryocooler, which is accompanied by a host of empirical correction factors, especially vis-à-vis the heat exchanger geometry could now be superseded.

2. Geometry models

2.1. Capillary tube

The geometry models of the helical tube and fins are derived and presented below. The notations are shown in Figs. 2 and 3. The locus of the helical tube could be expressed as follows:

$$\mathbf{r} = a\cos\theta\hat{\mathbf{i}} + a\sin\theta\hat{\mathbf{j}} + b\theta\hat{\mathbf{k}} \tag{1}$$

$$\hat{\mathbf{r}} = \frac{1}{\sqrt{a^2 + (b\theta)^2}}(a\cos\theta\hat{\mathbf{i}} + a\sin\theta\hat{\mathbf{j}} + b\theta\hat{\mathbf{k}}) \tag{2}$$

$$\hat{\mathbf{T}} = \frac{1}{\sqrt{a^2 + b^2}}(-a\sin\theta\hat{\mathbf{i}} + a\cos\theta\hat{\mathbf{j}} + b\hat{\mathbf{k}}) \tag{3}$$

$$\hat{\mathbf{n}} = \frac{1}{\sqrt{1 + (1+b)^2 + a^2(1+1/b)^2}}\Big\{[\cos\theta - (1+b)\sin\theta]\hat{\mathbf{i}} + [\sin\theta + (1+b)\cos\theta]\hat{\mathbf{j}} - [a(1+1/b^2)]\hat{\mathbf{k}}\Big\} \tag{4}$$

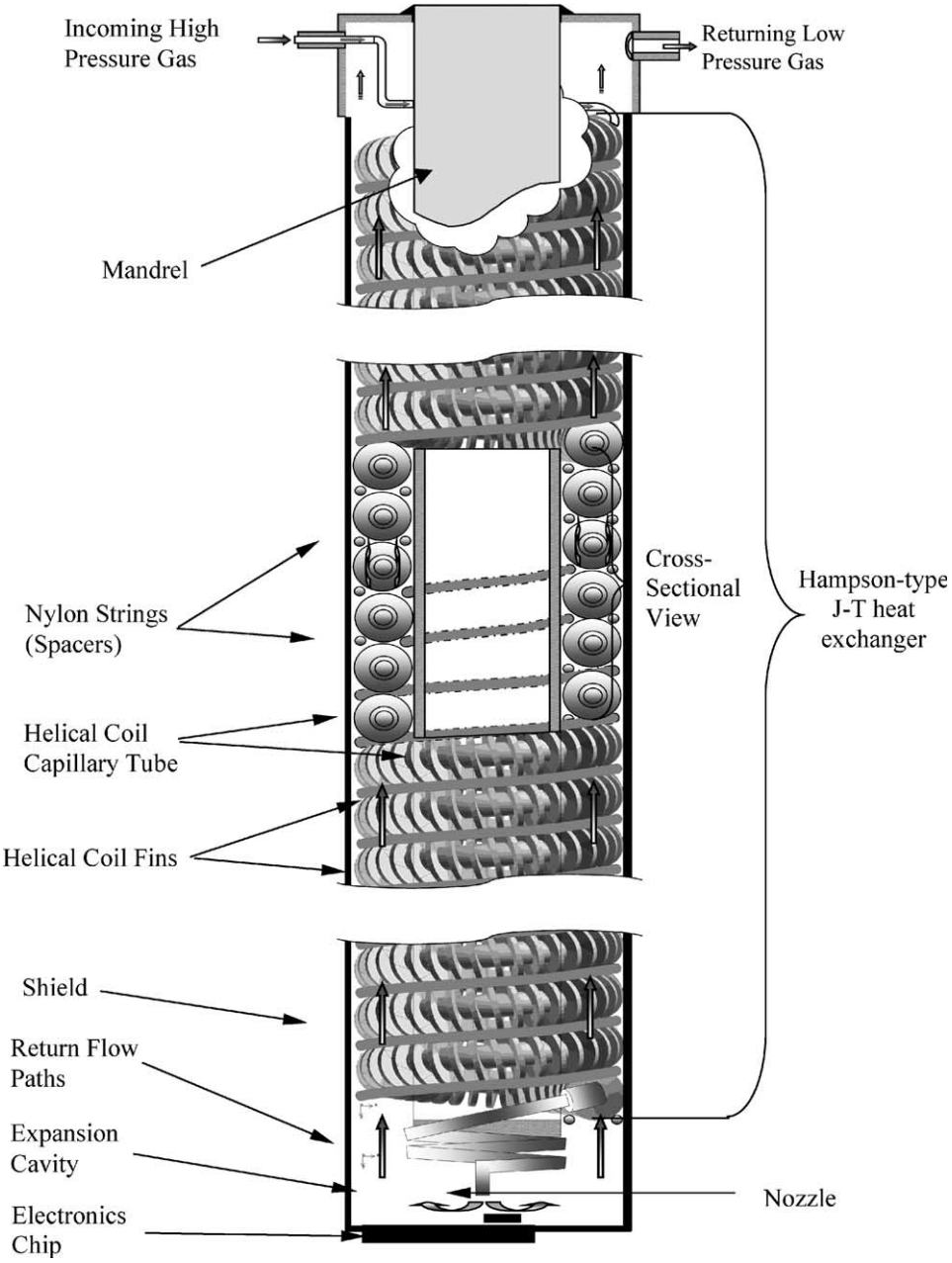

Fig. 1. Schematic of a typical Hampson type J–T cryocooler.

where $\hat{\mathbf{r}}, \widehat{\mathbf{T}}, \hat{\mathbf{n}}$ form an orthogonal system which traces the helical tube.

2.2. Fins

$$\hat{\mathbf{e}}_{\breve{\mathbf{r}}} = \cos\beta\,\hat{\mathbf{r}} + \sin\beta\,\hat{\mathbf{n}} \tag{5}$$

$$\hat{\mathbf{e}}_{\beta} = -\sin\beta\,\hat{\mathbf{r}} + \cos\beta\,\hat{\mathbf{n}} \tag{6}$$

$$\hat{\mathbf{e}}_{\breve{\mathbf{T}}} = \widehat{\mathbf{T}} \tag{7}$$

where $\hat{\mathbf{e}}_{\breve{\mathbf{r}}}, \hat{\mathbf{e}}_{\beta}, \hat{\mathbf{e}}_{\breve{\mathbf{T}}}$ form an orthogonal system which traces the helical fin.

Therefore at any $\widehat{\mathbf{T}}$, the locus of the helical fin is defined as

$$\mathbf{r}_{\text{fin}} = r\cos\beta\,\hat{\mathbf{r}} + r\sin\beta\,\hat{\mathbf{n}} \tag{8}$$

and its absolute location is described by

$$\mathbf{r}_{\text{2nd}} = \mathbf{r} + \mathbf{r}_{\text{fin}} \tag{9}$$

Alternatively it can be described as

$$\mathbf{r}_{\text{2nd}} = f_x\hat{\mathbf{i}} + f_y\hat{\mathbf{j}} + f_z\hat{\mathbf{k}} \tag{10}$$

Table 1
The dimensions of Hampson-type J–T cryocooler

Items	Specifications	
	Internal diameter (mm)	Outer diameter (mm)
Capillary tube, d_m	0.3	0.5
Mandrel, $d_{mandrel}$	2.3	2.5
Shield, d_{sh}	4.6	5.0
Diameter of spacer 1, d_{spc1}	0.2 mm	
Diameter of spacer 2, d_{spc2}	0.2 mm	
Helical pitch, b (or $Pitch_m$), of capillary tube	1.0 mm	
Fin height, H	0.25 mm	
Fin thickness, W_{fin}	0.1 mm	
Fin pitch, $Pitch_{fin}$	0.3 mm	
Length of heat exchanger, L	50.0 mm	
Number of complete helical turns, n_m	50	
Number of fin turns in the control volume, n_{fin}	37	
Fin surface angle, α	0.38 rad	
Primary helical tube radius, a_m	2.0 mm	
Primary helical fin radius, a_{fin}	2.0 mm	
Primary helical spacer 1 radius, a_{spc1}	1.35 mm	
Primary helical spacer 2 radius, a_{spc2}	2.65 mm	

where

$$f_x = a\cos\theta + \frac{r\cos\beta}{\sqrt{2+a^2/b^2}}(\cos\theta - \sin\theta) + \frac{r\sin\beta\left[-\frac{b+a^2/b}{2+a^2/b^2}\cos\theta - \left(b-\frac{b+a^2/b}{2+a^2/b^2}\right)\sin\theta\right]}{\sqrt{\left(\frac{b+a^2/b}{2+a^2/b^2}\right)^2 + \left(b-\frac{b+a^2/b}{2+a^2/b^2}\right)^2 + a^2\left[1-\frac{1}{b}\left(\frac{b+a^2/b}{2+a^2/b^2}\right)\right]^2}} \quad (11)$$

$$f_y = a\sin\theta + \frac{r\cos\beta}{\sqrt{2+a^2/b^2}}(\cos\theta + \sin\theta) + \frac{r\sin\beta\left[-\frac{b+a^2/b}{2+a^2/b^2}\sin\theta + \left(b-\frac{b+a^2/b}{2+a^2/b^2}\right)\cos\theta\right]}{\sqrt{\left(\frac{b+a^2/b}{2+a^2/b^2}\right)^2 + \left(b-\frac{b+a^2/b}{2+a^2/b^2}\right)^2 + a^2\left[1-\frac{1}{b}\left(\frac{b+a^2/b}{2+a^2/b^2}\right)\right]^2}} \quad (12)$$

$$f_z = b\theta - \frac{a}{b}\frac{r\cos\beta}{\sqrt{2+a^2/b^2}} - \frac{r\sin\beta\left[a-\frac{a}{b}\left(\frac{b+a^2/b}{2+a^2/b^2}\right)\right]}{\sqrt{\left(\frac{b+a^2/b}{2+a^2/b^2}\right)^2 + \left(b-\frac{b+a^2/b}{2+a^2/b^2}\right)^2 + a^2\left[1-\frac{1}{b}\left(\frac{b+a^2/b}{2+a^2/b^2}\right)\right]^2}} \quad (13)$$

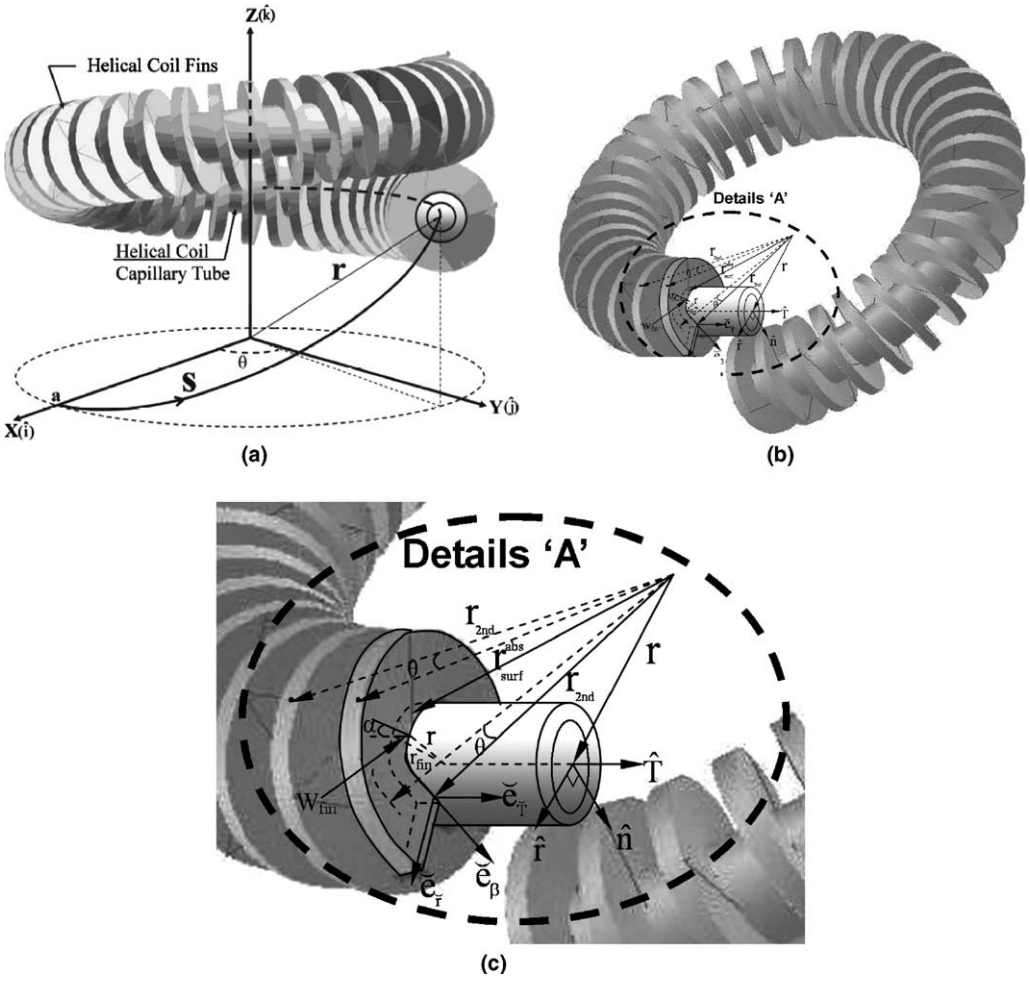

Fig. 2. Helical coil notations.

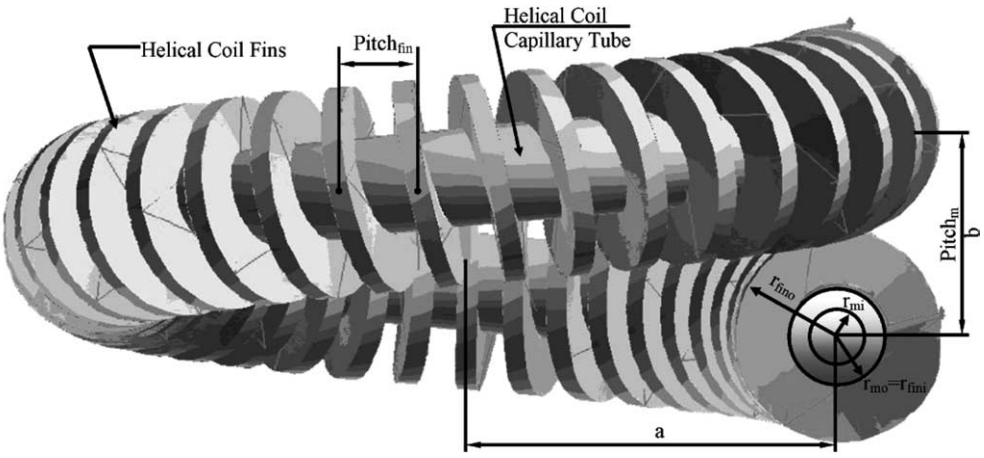

Fig. 3. Elevation view of the helical coil capillary tube and fins.

The related Jacobian is

$$J_m = \left| \left[\frac{\partial(f_x)}{\partial \beta} \cdot \frac{\partial(f_y)}{\partial r} - \frac{\partial(f_y)}{\partial \beta} \cdot \frac{\partial(f_x)}{\partial r} \right] \right| \tag{14}$$

where $f_z =$ constant and the relationship between θ and β is defined as

$$\beta - \beta_0 = \frac{\theta - \theta_0}{\Delta\theta} \cdot 2\pi = \frac{2\pi \cdot (\theta - \theta_0) \cdot \sqrt{a^2 + b^2}}{\text{Pitch}_{fin}} \tag{15}$$

where

$$\Delta\theta = \text{Pitch}_{fin} / \sqrt{a^2 + b^2} \text{ and } \beta_0 = 0 \quad \text{when} \quad \theta_0 = 0 \tag{16}$$

The surface of the helical fin is described as

$$\mathbf{r}_{surf} = r_{fin} \cos\beta \hat{\mathbf{r}} + r_{fin} \sin\beta \hat{\mathbf{n}} + (r_{fin} - r_{mo}) \tan\alpha \widehat{\mathbf{T}} \tag{17}$$

where

$$r_{mo} \leqslant r_{fin} \leqslant W_{fin} \cos\alpha + r_{mo} \tag{18}$$

Hence its absolute description is given by,

$$\mathbf{r}^{abs}_{surf} = a\cos\theta \hat{\mathbf{i}} + a \sin\theta \hat{\mathbf{j}} + b\theta \hat{\mathbf{k}} + \mathbf{r}_{surf} \tag{19}$$

Fig. 3 demonstrates the elevation view of the helical coil tube and fins calculated from the above model. The corresponding heat transfer surface areas for the thermodynamic model could be computed according to this model as tabulated in Table 2.

3. Thermodynamic model

To analyze the performance of a Hampson-type Joule–Thomson (J–T) cryocooler, the mathematical model which incorporates the geometry model of the recuperated heat exchanger is proposed. The governing equations consist of the energy balance, conservation of mass, thermal conduction and radiation between different components. They are listed in the following sections.

3.1. High pressure refrigerant in the helical capillary tube

Since the capillary tube diameter is much smaller than the capillary tube length, ≈1–1840, one-dimension steady state flow is assumed. The conservation of mass of the high pressure refrigerant inside the helical capillary tube could be expressed as

$$\frac{d\dot{m}_f}{ds} = 0 \tag{20}$$

Since the cryogen is compressible, the continuity equation is defined as

$$\rho_f \frac{\partial u_f}{\partial s} + u_f \frac{\partial \rho_f}{\partial s} = 0 \tag{21}$$

The refrigerant pressure inside the capillary tube drops rapidly due to the high velocity and viscosity of the refrigerant. The pressure drop along the natural helical direction (or the s-direction) of the capillary tube is given by

$$\frac{dp_f}{ds} = -\frac{2f_f \rho_f u_f^2}{D_{mi}} - \frac{d(\rho_f u_f^2)}{ds} \tag{22}$$

where for a compressible fluid,

$$\frac{d\rho_f(T_f, p_f)}{ds} = \frac{\partial \rho_f}{\partial T_f} \frac{dT_f}{ds} + \frac{\partial \rho_f}{\partial p_f} \frac{dp_f}{ds} \tag{23}$$

The fanning friction factor for the flow inside a helical coil is suggested by Timmerhaus [7] and Flynn [8] as follows:

$$f_f(p_f, T_f) = 0.184 \left(1.0 + 3.5 \frac{D_{mi}}{D_{Hx}}\right) Re(p_f, T_f)^{-0.2} \tag{24}$$

The cryogen temperature varies along the capillary tube due to the pressure drop, frictional loss and heat transfer between the gas and the tube wall. It is expressed as

$$h_f(T_m - T_f)\pi D_{mi} = G_f A_f \left[c_{pf} \frac{dT_f}{ds} + \left(v_f - T_f \frac{\partial v_f}{\partial T_f} \right) \frac{dp_f}{ds} + \frac{d(u_f^2/2)}{ds} \right] \tag{25}$$

where the heat transfer coefficient between the tube and gas is proposed by Timmerhaus [7] and Flynn [8] as

Table 2
Heat transfer specifications and areas

Descriptions	Expression
Control volume length, ds	$\mathrm{d}s = \sqrt{(\mathrm{Pitch}_{\mathrm{fin}}/2\pi)^2 + R_{\mathrm{curve}}^2} \Big/ (\mathrm{Pitch}_{\mathrm{fin}}/2\pi)$
Fin length in control volume, d fin	$\mathrm{d\,fin} = 2\pi n_{\mathrm{fin}} \sqrt{(\mathrm{Pitch}_{\mathrm{fin}}/2\pi)^2 + (D_{\mathrm{mo}}/2)^2}$
Total length of capillary tube	$L_{\mathrm{s}} = n_{\mathrm{m}} \cdot \mathrm{d}s$
Total length of fins	$L_{\mathrm{fin}} = n_{\mathrm{m}} \cdot \mathrm{d\,fin}$
Total cross-sectional area of shield excluding mandrel core in dz direction	$A_{\mathrm{Tot}} = \pi(D_{\mathrm{si}}^2 - D_{\mathrm{mandrel}}^2)/4$
Cross-sectional area of capillary tube in dz direction[a]	$A_{\mathrm{m}} = \int_0^{r_{\mathrm{mi}}} \int_0^{2\pi} J_{\mathrm{m}}\,\mathrm{d}\beta\,\mathrm{d}r$
Cross-sectional area of spacer 1 in dz direction[a]	$A_{\mathrm{spc1}} = \int_0^{r_{\mathrm{spc1}}} \int_0^{2\pi} J_{\mathrm{m}}\,\mathrm{d}\beta\,\mathrm{d}r$
Cross-sectional area of spacer 2 in dz direction[a]	$A_{\mathrm{spc2}} = \int_0^{r_{\mathrm{spc2}}} \int_0^{2\pi} J_{\mathrm{m}}\,\mathrm{d}\beta\,\mathrm{d}r$
Cross-sectional area of fins in dz direction[a]	$A_{\mathrm{fin}} = \int_{r_{\mathrm{fini}}}^{r_{\mathrm{fino}}} J_{\mathrm{m}}\,\mathrm{d}\beta\,\mathrm{d}r$
Cross-sectional area of return fluid flow in dz direction	$A_{\mathrm{l}} = A_{\mathrm{Tot}} - A_{\mathrm{m}} - A_{\mathrm{spc1}} - A_{\mathrm{spc2}} - A_{\mathrm{fin}}$
Hydraulic diameter of return fluid,[b] $D_{\mathrm{Hx}} = 4A_{\mathrm{l}}/[\pi(D_{\mathrm{si}} + D_{\mathrm{mandrel}}) + L_{\mathrm{spc1}} + L_{\mathrm{spc2}} + L_{\mathrm{m}} + L_{\mathrm{fin}}]$	
where $L_{\mathrm{spc1}} = \int_0^{2\pi} \sqrt{f_x^2 + f_y^2}\,\mathrm{d}\beta$, f_z = constant and $r = r_{\mathrm{spc1}}$	
$L_{\mathrm{spc2}} = \int_0^{2\pi} \sqrt{f_x^2 + f_y^2}\,\mathrm{d}\beta$, f_z = constant and $r = r_{\mathrm{spc2}}$	
$L_{\mathrm{m}} = \int_0^{2\pi} \sqrt{f_x^2 + f_y^2}\,\mathrm{d}\beta$, f_z = constant and $r = r_{\mathrm{m}}$	
$L_{\mathrm{fin}} = \int_{\beta_1}^{\beta_2} \sqrt{f_x^2 + f_y^2}\,\mathrm{d}\beta$, f_z = constant, $r = r_{\mathrm{fin}}$, $0 \leqslant \beta \leqslant 2\pi$ and $\beta_1 > \beta_2$	
Contact area between fluid and capillary tube per ds	$A_{\mathrm{fm}} = \pi D_{\mathrm{mi}} \cdot \mathrm{d}s$
Contact area between fins and capillary tube per ds	$A_{\mathrm{finm}} = \mathrm{d\,fin} \cdot W_{\mathrm{fin}}$
Contact area between return fluid and capillary tube per ds	$A_{\mathrm{ml}} = \pi D_{\mathrm{mo}} \cdot \mathrm{d}s - \mathrm{d\,fin} \cdot W_{\mathrm{fin}}$
Contact area between fins and return fluid per ds	$A_{\mathrm{finl}} = \left[2\pi n_{\mathrm{fin}} \sqrt{(\mathrm{Pitch}_{\mathrm{fin}}/2\pi)^2 + (D_{\mathrm{mo}}/2 + H_{\mathrm{fin}})^2} + \mathrm{d\,fin}\right] H_{\mathrm{fin}} + 2\pi n_{\mathrm{fin}} W_{\mathrm{fin}} \sqrt{(\mathrm{Pitch}_{\mathrm{fin}}/2\pi)^2 + (D_{\mathrm{mo}}/2)^2}$
Area of fluid flow in capillary tube along ds direction	$A_{\mathrm{f}} = \pi D_{\mathrm{mi}}^2/4$
Cross-sectional area of capillary tube along ds direction	$A_{\mathrm{m}} = \pi(D_{\mathrm{mo}}^2 - D_{\mathrm{mi}}^2)/4$
Cross-sectional area of fins along ds direction	$A_{\mathrm{fin}} = W_{\mathrm{fin}} \cdot H_{\mathrm{fin}}$
Total area of shield	$A_{\mathrm{si}} = \pi(D_{\mathrm{so}}^2 - D_{\mathrm{si}}^2)/4$

[a] J_{m} is obtained from Eq. (14).
[b] f_x,f_y,f_z stem from Eqs. (11)–(13), respectively.

$$h_{\mathrm{f}} = 0.023 c_p G_{\mathrm{f}} Re^{-0.2} Pr^{-2/3} \left(1.0 + 3.5 \frac{D_{\mathrm{mo}}}{D_{\mathrm{Hx}}}\right) \tag{26}$$

3.2. Helical capillary tube

The energy balance equation for the helical capillary tube can be expressed as

$$\frac{\mathrm{d}^2 T_{\mathrm{m}}}{\mathrm{d}s^2} = -\frac{h_{\mathrm{f}}(T_{\mathrm{m}} - T_{\mathrm{f}})(A_{\mathrm{fm}}/\mathrm{d}s)}{A_{\mathrm{m}} k_{\mathrm{m}}} - \frac{h_{\mathrm{l}}(T_{\mathrm{m}} - T_{\mathrm{l}})(A_{\mathrm{ml}}/\mathrm{d}s)}{A_{\mathrm{m}} k_{\mathrm{m}}} - \frac{2k_T(T_{\mathrm{m}} - T_{\mathrm{fin}})(A_{\mathrm{finm}}/\mathrm{d}s)}{A_{\mathrm{m}} k_{\mathrm{m}}} \tag{27}$$

where

$$k_T = \frac{k_{\mathrm{m}} \cdot k_{\mathrm{fin}}}{k_{\mathrm{fin}} \cdot W_{\mathrm{fin}} + k_{\mathrm{m}} \cdot H_{\mathrm{fin}}} \tag{28}$$

3.3. Helical fins

The energy balance equation for the helical fins around the helical capillary tube can be expressed as

$$\frac{d^2T_{fin}}{ds^2} = -\frac{h_l(T_{fin}-T_l)(A_{finl}/ds)}{A_{fin}k_{fin}} - \frac{2k_T(T_{fin}-T_m)(A_{finm}/ds)}{A_{fin}k_{fin}} \tag{29}$$

where the heat transfer coefficient [8] for the external return gas could be expressed as

$$h_l = 0.26c_pG_lRe^{-0.4}Pr^{-2/3} \tag{30}$$

3.4. Shield

The energy balance equation for the shield could be written as

$$\frac{d^2T_{sh}}{dz^2} = -\frac{h_l(T_{sh}-T_l)\pi D_{si}}{A_{si}k_{sh}} - \frac{h_r\pi D_{si}(T_{sh}^4-T_{amb}^4)}{A_{si}k_{sh}} \tag{31}$$

The radiative heat transfer coefficient [8] between the ambient temperature external enclosure and the shield is given as

$$h_r = \frac{\sigma}{1/\varepsilon_{sh} + (A_{sh}/A_{amb})(1/\varepsilon_{encl}-1)} \tag{32}$$

where ε_{sh} and ε_{amb} are respectively 0.048 and 0.08. $A_{sh}/A_{amb} \approx D_{sh}\Delta z/D_{encl}\cdot L$, with D_{amb} being 20 mm.

3.5. External return gas

The mass conservation of the external return gas along the outside fins is expressed as

$$\frac{d\dot{m}_l}{dz} = 0 \tag{33}$$

It is a compressible fluid and the continuity equation is cast as

$$\rho_l\frac{\partial u_l}{\partial z} + u_l\frac{\partial \rho_l}{\partial z} = 0 \tag{34}$$

The momentum equation of the return gas along the primary axial direction (or the z-direction) of the helical capillary tube and fins could be written as

$$-\frac{dp_l}{dz} = \frac{2f_l\rho_l u_l^2}{D_{Hl}} + \frac{d(\rho_l u_l^2)}{dz} \tag{35}$$

where

$$\frac{d\rho_l(T_l,p_l)}{dz} = \frac{\partial\rho_l}{\partial T_l}\frac{dT_l}{dz} + \frac{\partial\rho_l}{\partial p_l}\frac{dp_l}{dz} \tag{36}$$

The energy balance equation of the return gas along the primary axial direction (or the z-direction) of the heat exchanger is represented by

$$h_l(T_l-T_m)\frac{A_{ml}}{dz} + h_l(T_l-T_{fin})\frac{A_{finl}}{dz} + h_l(T_l-T_{sh})\pi D_{si} = G_lA_l\left[c_{pl}\frac{dT_l}{dz} + \left(v_l - T_l\frac{dv_l}{dT_l}\right)\frac{dp_l}{dz} + \frac{d(u_l^2/2)}{dz}\right] \tag{37}$$

where the fanning friction factor for the return gas is given as [8]

$$f_l(p_l,T_l) = 0.184Re(p_l,T_l)^{-0.2} \tag{38}$$

The conversion factor between ds and dz is given by,

$$\frac{ds}{dz} = \frac{\sqrt{(\text{Pitch}_m/2\pi)^2 + R_{curve}^2}}{\text{Pitch}_m/2\pi} \tag{39}$$

3.6. Spacers

Nylon strings, which possess an extremely low thermal conductivity, are wound round the helical capillary tube and fins to ensure that the returning low pressure gas only flows pass, and thereby enhancing its contact with, the fins and the primary helical capillary tube. In our model the cross-sectional area occupied by the spacers is consistently calculated according to the geometry model. This provides an accurate evaluation of the flow cross-sectional area and the affiliated heat transfer surface area.

3.7. Entropy generation for the internal fluid

The entropy generation equation is used to assess the choking position of the high pressure gas in the capillary tube and is expressed as

$$\frac{d\dot{S}_{gen}}{ds} = \dot{m}_f\left\{\frac{1}{T_f}\left[c_{pf}\frac{dT_f}{ds} + \left(\frac{1}{\rho_f} + \frac{T_f}{\rho_f^2}\frac{d\rho_f}{dT_f}\right)\frac{dp_f}{ds}\right] - \frac{1}{\rho_fT_f}\frac{dp_f}{ds}\right\} - h_f\left(\frac{T_m-T_f}{T_m}\right)\cdot\frac{A_{fm}}{ds} \geqslant 0. \tag{40}$$

3.8. Jet impingement boiling

The jet impingement boiling correlation on a heated surface [9] is used to estimate the heat flux at the load

$$Q/A = 181.146(\Delta T)^{1.218} \tag{41}$$

where ΔT is the temperature difference between the surface and the measured bulk fluid.

3.9. Performance calculation

The coefficient of performance (COP) of the heat exchanger, for an ideal cryocooler, is defined as

$$\text{COP}_i = \frac{h_5-h_1}{T_5(s_5-s_1)-(h_5-h_1)} \tag{42}$$

whereas for a practical cryocooler, it could be represented as

$$\text{COP} = \frac{h_5-h_1}{T_5(s_5-s_1)-(h_5-h_1)+c_p(T_5-T_{5'})} \tag{43}$$

Table 3
Thermal conductivities of materials

Materials	Correlation	Relative errors [11]
Copper (fins)	$k_{\text{fin}} = \begin{cases} 0.2413T^2 - 47.775T + 2848, (60\text{K} \leqslant T \leqslant 100\text{K}) \\ 0.028T^2 - 1.525T + 608, (100\text{K} \leqslant T \leqslant 300\text{K}) \end{cases}$	<1.5%
Monel (shield)	$k_{\text{sh}} = 6.5169 \ln T - 14.76, (40\text{K} \leqslant T \leqslant 400\text{K})$	<1.0%
Stainless steel (capillary tube)	$k_{\text{m}} = 5.0353 \ln T - 13.797, (40\text{K} \leqslant T \leqslant 400\text{K})$	<1.0%

The corresponding figure of merit (FOM) is given by

$$\text{FOM} = \frac{\text{COP}}{\text{COP}_i} \tag{44}$$

The effectiveness of the heat exchanger is commonly defined as [8]

$$\varepsilon = \frac{h_{5'} - h_4}{h_5 - h_4} \tag{45}$$

The liquefied yield fraction of the heat exchanger is given by [8]

$$y = \frac{(h_5 - h_1) - (1 - \varepsilon)(h_5 - h_4)}{(h_5 - h_{\text{f}}) - (1 - \varepsilon)(h_5 - h_4)} \tag{46}$$

3.10. Physical properties of the cryogen and materials

Argon is chosen as the cryogen due to its easy availability, low cost and being able to achieve a relatively low cryogenic temperature. The thermophysical properties of argon are obtained from NIST [10] which makes use of the Helmholtz energy equation, a modified Benedict–Webb–Rubin equation (mBWR), and an extended corresponding states model (ECS). The viscosity and thermal conductivity values are determined with a fluid specific model and a variation of the ECS method.

Temperature dependent thermal conductivities of copper, monel, stainless steel and polycarbonate are used in the simulation. Copper is used for the fins that are wound round the stainless steel capillary tube. In the experiments from which we obtain the performance data to validate our model [5,6], the assembly is inserted into a monel shield and insulated with polycarbonate. Dewar is favored in actual applications and can be readily analyzed by our simulation. The exterior of the polycarbonate is assumed to be perfectly insulated in our model. The relevant empirical correlations are summarized in Table 3 [8,11].

4. Results and discussion

This simulation was applied to a Hampson-type Joule–Thomson (J–T) cryocooler which is shown in Fig. 1 and its dimensions are delineated in Table 1.

Figs. 3 and 4 feature the elevation view of the helical coil capillary tube and fins and the cross-sectional view of the J–T cryocooler respectively as obtained from the geometry model. This provides the real locus of the helical coil tube and fins and helps designers to better understand the Hampson-type J–T heat exchanger. The heat and mass transfer surface area and the cross-section area could therefore be accurately calculated. This eliminates the estimation and adjustment for the surface area and flow hydraulic diameter which has been used in some previous works [5,6].

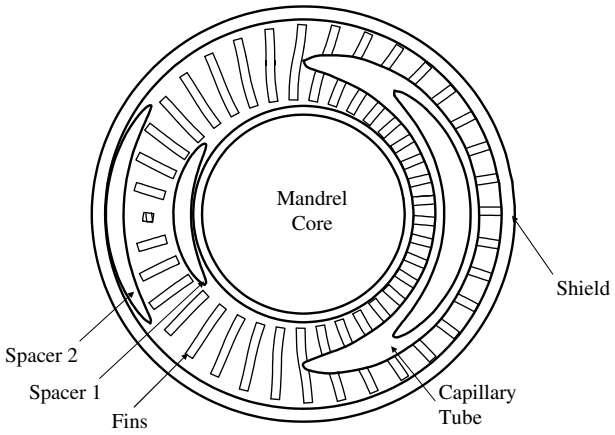

Fig. 4. Cross-sectional view of the J–T cryocooler.

The simulation results are compared with the experimental data [6] as shown in Table 4. In our simulation, the heat exchanger inlet pressure, nozzle outlet pressure and the corresponding saturated temperature are used as input to the computation. Only the relative errors of the outlet temperatures of the return gas are compared with the simulated results. This is due to the unavailability of tiny sensors to measure the pressures and temperatures within the capillary tube. It is noted that the measured return gas outlet temperature is slightly higher than the simulated results. This could be due to: (i) the use of the polycarbonate instead of a Dewar flask, which inevitably increases the heat gain during the experiment; (ii) readings of the temperature sensor at the return gas outlet are affected by the ambient conditions on account of the minuteness of the exit port. However, it is observed that the relative errors between the simulations and experiments all fell within 3%.

Fig. 5 shows the simulated temperature–entropy diagram of the cryogen in the cryocooler. The trend is similar to a typical T–S chart [8]. However, we find that the pressure drops much more rapidly in the high pressure gas channel due to the higher frictional loss and expansion

Table 4
A comparison between the experimental data [6] and simulation results

Case	Pressure (bar)		Temperature (K)		M_v (SLPM)	Temperature (T_{outlet}, K)		Relative error (%)
	p_1	p_3	T_{inlet}	$T_{sat} = f(p_3)$		Experiment	Simulation	
1	179.12	1.7272	291.49	92.68	13.927	282.57	276.93	2.00
2	169.86	1.7460	291.40	92.80	13.102	283.73	277.12	2.33
3	160.10	1.6362	292.25	92.11	12.060	284.77	278.53	2.19
4	149.66	1.4713	292.14	90.99	10.948	284.90	279.20	2.00
5	140.47	1.3426	291.94	90.06	10.145	284.98	279.34	1.98

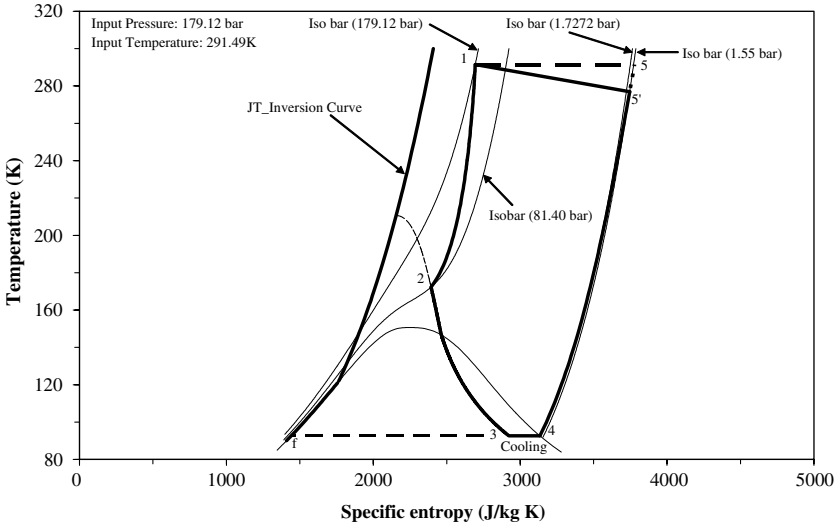

Fig. 5. A T–s diagram of the Hampson-type J–T cryocooler.

process than in the low pressure channel. This in turn increases the cooling capacity of the Hampson-type Joule–Thomson (J–T) cryocooler and demonstrates the efficacy of the recuperative method in substantially improving its performance. The Joule–Thomson (J–T) inversion curve has also been plotted into the chart. To the right of the curve is where the cooling process occurs.

Fig. 6 presents the effect of the load temperature on the cooling capacity. With an increase in the cooling load temperature, the cooling capacity increases greatly. This corroborates with the basic theory commonly used in the traditional air-conditioning and refrigerant systems. It is noted that the cooling capacity is almost linearly proportional to the load temperature.

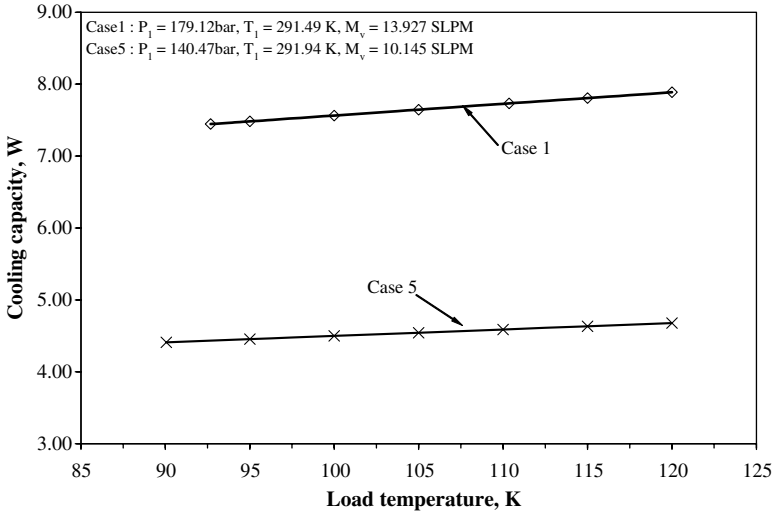

Fig. 6. Effect of the load temperature on the cooling capacity.

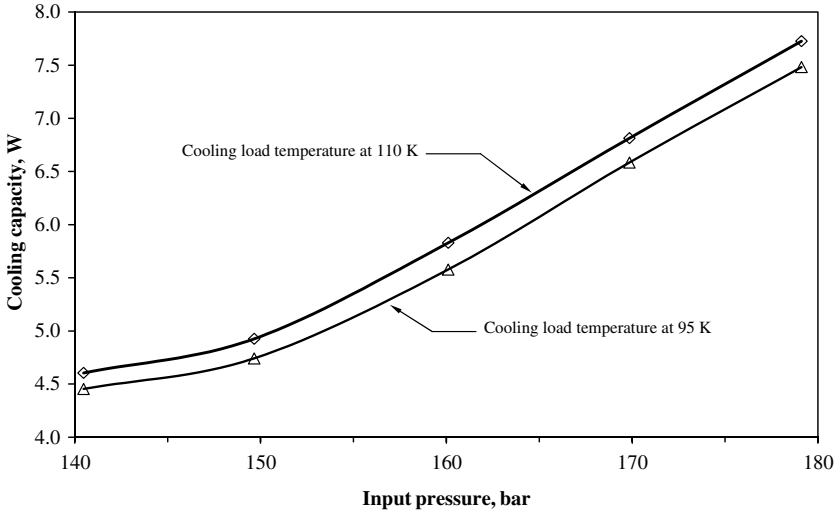

Fig. 7. Effect of the input pressure on the cooling capacity.

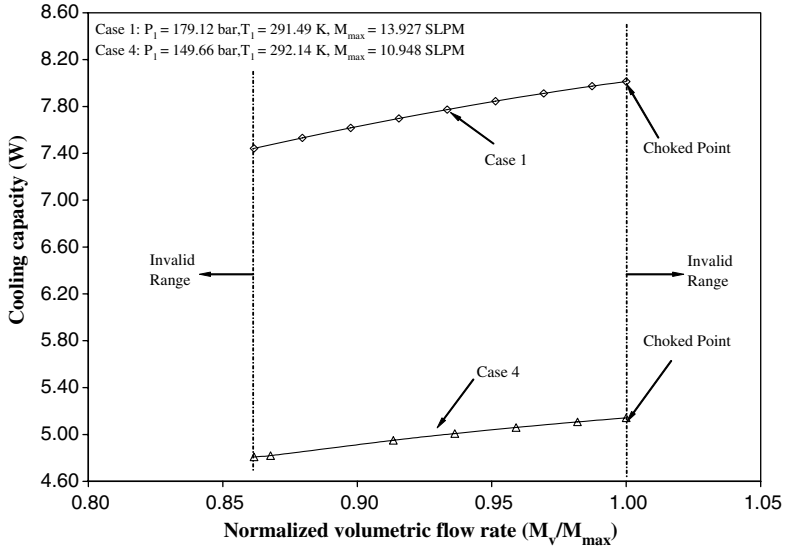

Fig. 8. Effect of the cryogen volumetric flow rate on the cooling capacity.

The higher the heat exchanger inlet pressure, the higher the cooling capacity that could be achieved. This is evident from the simulation results as shown in Fig. 7. Within our simulated range, the cooling capacity increases with the inlet pressure. It is observed from the chart that the cooling capacity increases gently at the lower pressure range while it increases more rapidly at the higher range.

Fig. 8 shows the effect of the cryogen flow rate on the cooling capacity. Within the valid range as considered in our simulation, the higher the flow rate supplied to the heat exchanger, the higher the achievable cooling capacity. The choked point happens when the local entropy generation equals zero and the entropy generation becomes negative when liquid phase exists. This figure effectively demonstrates the ability of our formalism in ascertaining the maximum cryogen flow rate based on a set of given heat exchanger specifications.

The COPs and FOMs of the Hampson-type J–T cryocooler at different inlet pressures and the corresponding maximum cryogen flow rates are plotted in Fig. 9. It is clear that these two parameters improve with the inlet pressure.

Fig. 10 shows the variations of effectiveness and liquefied yield fractions under different inlet pressures. It is shown from the chart that:

(i) the Hampson-type J–T cryocooler have relatively low yields with only about 10% of the circulated gas becoming liquid,
(ii) the liquefied yield fraction increases with the input pressure,
(iii) the cryocooler effectiveness decreases as the input pressure increases, and
(iv) the liquefied yield fraction is sensitive to the heat exchanger effectiveness.

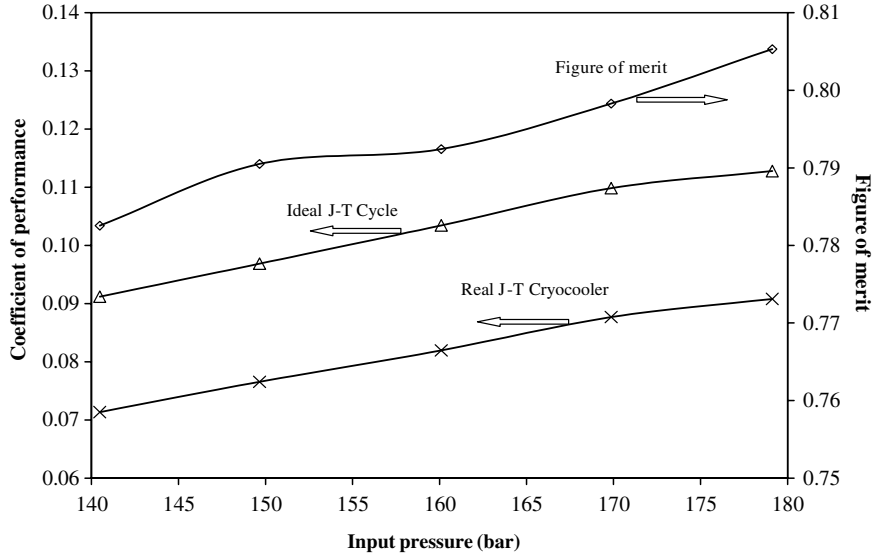

Fig. 9. Coefficients of performance and figures of merit under different inlet pressures.

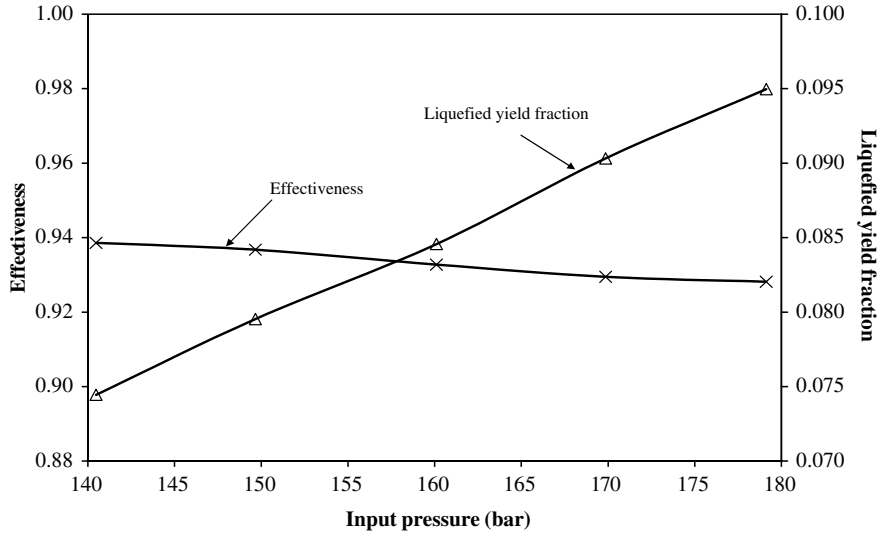

Fig. 10. Variation of the effectiveness and liquefied yield fraction with different inlet pressures.

5. Conclusions

A geometry model of the recuperative heat exchanger of the Hampson-type J–T cryocooler has been formulated and it accurately reproduces the actual locus of the double helical tube and fins. Based on this, the simulation design tool for a Hampson-type Joule–Thomson (J–T) cooler has been developed to predict and analyze the performance of such cryocoolers. The result shows that the numerical simulation agrees well with the experimental data. The performance characteristics of a Hampson-type Joule–Thomson (J–T) cooler are analyzed and discussed. Our formalism is therefore useful for the prediction, estimation and evaluation of the Hampson-type J–T coolers. It provides realistic design solutions for manufacturers and avoid most of the "trial and error" procedures commonly adopted.

References

[1] B.Z. Maytal, Performance of ideal flow regulated Joule–Thomson cryocooler, Cryogenics 34 (1994) 723–726.
[2] F.C. Chou, S.M. Wu, C.F. Pai, Prediction of final temperature following Joule–Thomson expansion of nitrogen gas, Cryogenics 33 (1993) 857–862.
[3] F.C. Chou, S.B. Chien, Preliminary experimental and numerical study of transient characteristics for a Joule–Thomson cryocooler, Cryogenics 35 (1995) 311–316.
[4] S.B. Chien, L.T. Chen, F.C. Chou, A study on the transient characteristics of a self-regulating Joule–Thomson cryocooler, Cryogenics 36 (1996) 979–984.

[5] H. Xue, K.C. Ng, J.B. Wang, Performance evaluation of the recuperative heat exchanger in a miniature Joule–Thomson cooler, Applied Thermal Engineering 21 (2001) 1829–1844.
[6] K.C. Ng, H. Xue, J.B. Wang, Experimental and numerical study on a miniature Joule–Thomson cooler for steady-state characteristics, International Journal of Heat and Mass Transfer 45 (2002) 609–618.
[7] K.D. Timmerhaus, T.M. Flynn, Cryogenic Process Engineering, Plenum Press, New York, USA, 1989.
[8] M.T. Flynn, Cryogenic Engineering, Marcel Dekker Inc., NewYork, 1997.
[9] A. Brian, S. Sherman, H. Schwartz, Jet impingement boiling using a J–T cryostat, ASME, Cryogenic Heat Transfer 167 (1991) 11–17.
[10] E.W. Lemmon, A.P. Peskin, M.O. McLinden, D.G. Friend, Thermodynamic and transport properties of pure fluids, NIST Standard Reference Database 12, Version 5.0 (2000).
[11] R.H. Perry, D.W. Green, J.O. Maloney, Perry's Chemical Engineers' Handbook, McGraw-Hill, New York, 1997, pp. 2-318–2-337.